Towards Efficient Integration of Information and Energy Reception

Sotiris A. Tegos, *Student Member, IEEE,* Panagiotis D. Diamantoulakis, *Senior Member, IEEE,* Koralia N. Pappi, *Member, IEEE,* Paschalis C. Sofotasios, *Senior Member, IEEE,* Sami Muhaidat, *Senior Member, IEEE,* and George K. Karagiannidis, *Fellow, IEEE*

***Abstract*—One of the major goals of emerging wireless systems is to prolong the lifetime of wireless communication devices. To this end, this contribution evaluates and optimizes the performance of simultaneous wireless information and power transfer (SWIPT) with an integrated energy and information receiver, which has the advantage of low complexity and energy cost. A tractable expression for the achievable rate is first derived, which is subsequently used to quantify the achievable harvested energy−rate region for the two fundamental SWIPT protocols, namely power-splitting (PS) and time-switching (TS). In this context, the joint harvested energy−rate outage probability is then defined and minimized for a point-to-point and multicasting system, determining the optimal PS and TS factor for both a linear and a nonlinear energy harvesting model. Additionally, a TS-based broadcasting system is dynamically optimized by maximizing the energy harvested by all users under an achievable rate threshold for each user. The formulated optimization problem is, in fact, particularly challenging due to the non-convex form of the expression for the achievable rate. Yet, an effective solution is ultimately achieved by converting this problem into a convex one. Also, respective computer simulation results corroborate the effectiveness of the proposed framework. Overall, it is shown that the offered results provide meaningful theoretical and practical insights that will be useful in the design and efficient operation of wireless powered systems. Indicatively, unlike the trend in common separated receivers, a region has been identified where TS outperforms PS.**

***Index Terms*—Simultaneous wireless information and power transfer (SWIPT), integrated receiver, power-splitting, time-switching, joint harvested energy−rate outage probability.**

This work was supported in part by Khalifa University under Grant No. KU/RC1-C2PS-T2/8474000137 and Grant No. KU/FSU-8474000122, by Nokia Bell Labs through the global donation program for Wireless Powered Remote Patient Monitoring (SPRING), and by Greek General Secretariat for Research and Technology under Grant No. T6YBP-00134.

This work has been presented in part at the 19^{th} IEEE International Workshop on Signal Processing Advances in Wireless Communications (IEEE SPAWC '18), Kalamata, Greece, June 2018 [1].

S. A. Tegos, P. D. Diamantoulakis, and G. K. Karagiannidis are with the Department of Electrical and Computer Engineering, Aristotle University of Thessaloniki, 54 124, Thessaloniki, Greece (e-mails: {tegosoti; padiaman; geokarag}@auth.gr).

K. N. Pappi is with the Department of Electrical and Computer Engineering,Aristotle University of Thessaloniki, 54 124, Thessaloniki, Greece and also with Intracom S. A. Telecom Solutions, GR-57001, Thessaloniki, Greece (email: kpappi@auth.gr).

P. C. Sofotasios is with the Center for Cyber-Physical Systems, Department of Electrical and Computer Engineering, Khalifa University of Science and Technology, P. O. Box 127788, Abu Dhabi, UAE and also with the Department of Electrical Engineering, Tampere University, FI-33101, Tampere, Finland (e-mail: p.sofotasios@ieee.org).

S. Muhaidat is with the Center for Cyber-Physical Systems, Department of Electrical and Computer Engineering, Khalifa University of Science and Technology, PO Box 127788, Abu Dhabi, UAE and also with the Department of Electronic Engineering, University of Surrey, GU2 7XH, Guildford, UK (e-mail: muhaidat@ieee.org)

I. Introduction

EMERGING wireless technologies are largely characterized by versatile, yet stringent energy efficiency requirements of the involved devices. Therefore, wireless power transfer (WPT) constitutes a promising paradigm as it can ultimately increase the efficiency and lifetime of such devices [2]–[4]. This is particularly important in numerous applications including those relating to the Internet of Things (IoT), such as wearables and sensors networks, since energy harvesting (EH) can assist in achieving robust operation under realistic mobility requirements. Furthermore, low power devices, such as wireless sensor networks, can benefit significantly from EH since traditional batteries can be potentially replaced by super capacitors [2]. In fact, this is ultimately desirable since replacing or recharging the batteries of an increased number of devices is typically inconvenient, costly and even dangerous, particularly in remote areas, harsh industrial environments, and healthcare applications. Furthermore, EH can reduce the actual number of batteries needed for such off grid devices and, thus, counterbalance the corresponding environmental impact.

Nevertheless, the main drawback of basic EH methods is that they rely solely on ambient energy sources, such as solar, wind energy, and vibrations, which are largely uncontrollable and usually unpredictable. As a result, harvesting energy from sources that intentionally generate energy, such as radio frequency (RF) signals, turns out to be a more effective and interesting alternative. To this end, the potential to apply WPT, in wireless communication applications has recently received considerable attention [3]–[6]. However, WPT creates unique challenges in the design of communication systems since in some cases it conflicts with the corresponding information transmission. More specifically, nodes cannot harvest energy and receive information simultaneously, which complicates the design of communication systems with WPT [2], [7]. This is the main challenge of simultaneous wireless information and power transfer (SWIPT), which aims at unifying the information and energy transmission by also taking into account the inherent dependence on specific system implementations (see [8] and the references therein). In this framework, there are two main approaches according to which the users either: i) exploit the received power to sequentially transmit their information using the harvest-then-transmit protocol [9]–[15]; or ii) receive information while using part of the received energy to feed their receiver circuit and/or charge their batteries, which is also the core idea investigated in the present contribution.

In single-antenna nodes, the second approach can be performed by two fundamental techniques, namely power-splitting (PS) and time-switching (TS). PS is based on the division of the signal power into two streams, whereas in the TS, the received signal is used solely for harvesting energy or receiving information during specific time periods. In this context, the idea of PS and TS has been addressed in various case studies, such as one source-destination pair [16], [17], multiple-input multiple-output (MIMO) communications systems [18]–[25], orthogonal frequency division multiplexing (OFDM) [16], [17], [26], cooperative networks [27]–[32], and physical layer security based wireless communications [33]–[35]. In the majority of these works a linear model is used for energy harvesting. Nevertheless, in the recent works [36]–[40] a more realistic nonlinear EH model has been taken into consideration.

A. Motivation

It is recalled that in all aforementioned contributions on SWIPT the separated receiver is used for information decoding (ID) and EH. This receiver splits the signal immediately upon reception and there are two separated circuits for EH and ID. However, circuit power consumed by ID constitutes a considerable design issue for SWIPT systems, since the circuit power reduces the net harvested energy that can be stored in the battery. In particular, the active mixers used in conventional information receivers for down-conversion are highly power-consuming. Motivated by this, the seminal contribution in [41] proposed an architecture for the integrated information and energy receiver, where the rectifier that is used for EH is also used for RF band to direct current (DC) conversion. This substitutes the traditional down-conversion and as a result, this receiver architecture consumes less power by providing a dual use of the rectifier and avoiding the use of active devices, which is critical for low power consumption. In this context, this receiver necessitates the use of noncoherent modulation schemes [41], which reduces the overhead of channel estimation [42]. Also, the same receiver is considered in the recent contribution in [43], where sequential decoding under the effect of fading conditions is proposed, aiming at low-complexity detection and efficient memory utilization. Moreover, it was shown in [44] and [45] that the separated receiver can be combined with the integrated one to maintain both amplitude and phase information, at the expense of increased system complexity[1].

However, the investigation and optimization of the performance of such receiver architectures is cumbersome, e.g., in terms of outage probability, mainly due to the absence of an appropriate expression for the achievable rate. Furthermore, in the integrated receiver, the optimization of the PS factor is affected by the noise introduced by the involved analog-to-digital converter (ADC), which has also not been addressed comprehensively. Likewise, the performance of the integrated receiver in a TS system has not been investigated and compared with the PS counterpart, while the use of this receiver is limited for point-to-point communication scenarios, since it has not been extended to multiuser communication systems.

[1]This multi-branch architecture is out of the scope of the present contribution, which focuses on the integrated receiver.

B. Contribution

In the present analysis, a comprehensive theoretical framework is developed to facilitate the investigation of the achievable performance and behavior of the aforementioned integrated receiver. Besides the simplistic point-to-point case, a multicasting and a broadcasting system consisting of multiple users are also analyzed, where each user is equipped with an integrated receiver. Moreover, both PS and TS scenarios are investigated as the architecture of the integrated receiver differs from that of the separated receiver, where PS always outperforms TS. More specifically, the contributions of this work are listed below:

- We derive a tractable expression for the corresponding achievable rate, which accounts for both PS and TS strategies, allowing their performance comparison when used on systems with integrated receivers. In spite of focusing on point-to-point, multicasting and broadcasting cases, the derived expression is generic and can be also used for other communication scenarios. It is highlighted that this expression differs from the Shannon capacity, which is used in the separated receiver architecture.
- We introduce a novel and useful performance metric for integrated receivers, namely *joint harvested energy−rate outage probability*, which quantifies the tradeoff between energy and information transmission. This metric is evaluated for the point-to-point and multicasting cases taking into consideration both a linear and a nonlinear EH model. To this effect, it is subsequently minimized resulting in the optimization of the PS and TS factors and in specifying the optimal operating point in the determined harvested energy−rate region.
- We investigate a critical practical scenario for broadcasting, where each user has specific quality of service (QoS) requirements in terms of an achievable rate threshold. In this case, the non-convex problem of the dynamic maximization of the total harvested energy is defined and solved. The considered optimization problem is challenging mainly because of the complex expression of the achievable rate, compared with the separated receiver architecture.
- We provide extensive simulation results to present the harvested energy−rate region for the PS and TS systems. Also, the offered results illustrate the comparison of the considered systems in terms of the novel metric of joint harvested energy−rate outage probability, as well as the performance of the broadcasting system using dynamic optimization.

The offered theoretical and technical results are both insightful and useful, and to the best of the authors' knowledge they have not been previously reported in the open literature.

C. Structure

The rest of the paper is organized as follows: Section II describes the system model for a user equipped with the

aforementioned integrated receiver. In Section III, the expression of the harvested energy is presented and the tractable expression for the achievable rate is derived. Moreover, the considered TS system is compared with the PS counterpart and the achievable harvested energy−rate region is determined. In Section IV, the joint harvested energy−rate outage probability is defined, determined and minimized. Section V formulates the broadcasting optimization problem with specific user QoS requirements, which is optimally solved. In Section VI, simulation results are provided to corroborate the derived analytic results and to illustrate the performance of the considered systems. Finally, useful discussions and closing remarks are provided in Section VII.

II. System Model

We consider the downlink of a communication network, which consists of one base station (BS) that performs SWIPT to serve the assigned EH users. It is assumed that all nodes have a single antenna and each user is equipped with an integrated information and energy receiver. Moreover, perfect channel state information (CSI) is assumed, which is a common assumption in the relevant literature both for the case of separated [16]–[18], [20], [23], [46] and integrated receivers [41], [43], [45]. It is noted that in the integrated receiver architecture this assumption is more realistic compared to the one in separated receivers, because energy detection is carried out and, thus, only the amplitude of the transmitted signal is needed and not its phase [42]. In this context, the analysis focuses on three different communication systems, namely:

- Point-to-point communication.
- Downlink multicasting, where the BS transmits the same information (e.g., a common file) to N users simultaneously.
- Downlink broadcasting, where the BS needs to send independent information to each user.

When multiple users are assumed, i.e., in the last two systems, the notation $(\cdot)_n$ is used to denote the value of the variable $(\cdot)$ for the n-th user. In addition, the path loss factor between the BS and the user is denoted by l, while the small scale fading coefficient is given by the complex random variable $h \sim \mathcal{CN}(0,1)$. Also, two SWIPT strategies are considered in the sequel, i.e., PS and TS. A more detailed description of the application of these protocols on the integrated receiver is given in the following subsections.

A. Power-splitting

In the integrated receiver, which is shown in Fig. 1, when PS is used the received RF signal is converted to a DC signal by a rectifier consisting of a Schottky diode and a passive low pass filter. Then, the DC signal splits into two streams, one proportional to the PS factor $\rho \in [0,1]$ and one proportional to the factor $1-\rho$ for EH and ID, via energy detection [41], respectively.

Based on the above, the DC signal is represented as

$$i_{\text{DC}}(t) = \left| |h|\sqrt{lP}A(t) + n_A(t) \right|^2 + n_{\text{rec}}(t), \tag{1}$$

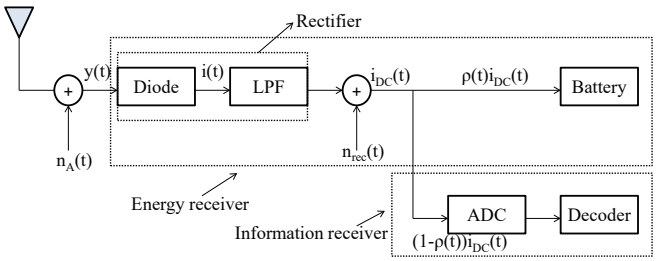

Fig. 1. Architecture of an integrated SWIPT PS receiver.

where $A(t)$ denotes the amplitude of the complex baseband signal at the transmitter side, P denotes the average transmit power, whereas $n_A(t) \sim \mathcal{CN}(0,\sigma_A^2)$ and $n_{\text{rec}} \sim \mathcal{N}(0,\sigma_{\text{rec}}^2)$ denote the additive noise introduced by the antenna and the rectifier, respectively.

As shown in [41], the portion of the DC signal for ID is processed by an ADC. Thus, the output of the noiseless power splitter and the ADC, $y_{\text{PS}}[k]$, is given by

$$y_{\text{PS}}[k] = (1-\rho)\left(\left| |h|\sqrt{lP}A[k] + n_A[k] \right|^2 + n_{\text{rec}}[k] \right) + n_{\text{ADC}}[k], \tag{2}$$

where k denotes discrete time and $n_{\text{ADC}} \sim \mathcal{N}(0,\sigma_{\text{ADC}}^2)$ denotes the additive noise introduced by the ADC.

Based on (2) and considering that the antenna noise is negligible ($\sigma_A^2 \to 0$), the equivalent discrete-time memoryless channel is modeled as

$$Y = l|h|^2 PX + Z, \tag{3}$$

where X denotes the signal power, which is the non-negative channel input, Y denotes the channel output and

$$Z \sim \mathcal{N}\left(0, \sigma_{\text{rec}}^2 + \frac{\sigma_{\text{ADC}}^2}{(1-\rho)^2}\right) \tag{4}$$

denotes the equivalent processing noise. It is noted here that $X \in \mathbb{R}^+$, which results from the utilization of the integrated receiver and more specifically from the dual use of the rectifier. Also, $\mathbb{E}[X] \leq 1$. The expression in (3) highlights the importance of the ADC noise since it becomes evident from (4) that ignoring this renders the equivalent channel output, Y, independent to the PS factor. Moreover, it does not necessarily hold that $\sigma_{\text{rec}}^2 > \sigma_{\text{ADC}}^2/(1-\rho)^2$, since the second term also depends on the PS factor. Hence, for relatively high values of ρ, its values become comparable or even higher than the value of the useful signal and the variance of the rectifier noise.

B. Time-switching

In the integrated receiver, which is shown in Fig. 2, when TS is used the received RF signal is again converted to a DC signal by the rectifier. This signal is then used for harvesting energy for the portion of time a, whereas for the portion $1-a$ it is used for decoding information.

The DC signal is the same as the one in the PS counterpart, which is therefore represented by (1). After the ADC, the

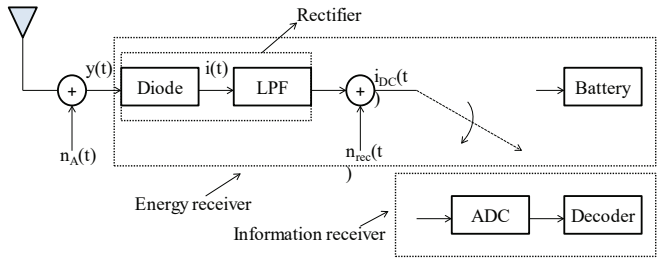

Fig. 2. Architecture of an integrated SWIPT TS receiver.

output $y_{\text{TS}}[k]$ is given by

$$y_{\text{TS}}[k]=\begin{cases} 0, & k \le a, \\ \left||h|\sqrt{lP}A[k]+n_A[k]\right|^2+n_{\text{rec}}[k]+n_{\text{ADC}}[k], & k > a. \end{cases} \tag{5}$$

Based on (5) and considering that the antenna noise is negligible, the equivalent discrete-time memoryless channel is given by (3), where $Z \sim \mathcal{N}\left(0, \sigma^2_{\text{rec}} + \sigma^2_{\text{ADC}}\right)$ is the equivalent processing noise.

III. Harvested Energy−Data Rate Tradeoff

In this section we derive the expressions of the harvested energy for a linear and a nonlinear EH model and the achievable rate for the point-to-point scenario in the considered setup.

A. Harvested Energy

1) Power-splitting: Regarding the linear EH model, it is assumed that the converted energy in the energy receiver is linearly proportional to i_{DC}, with a conversion efficiency $0 < \zeta \le 1$. It is also assumed that the harvested energy due to the equivalent processing noise is a negligible constant and, thus, it can be ignored. Hence, the harvested energy, which coincides with power assuming the symbol period to be one, in the case of PS is given by [41]

$$Q_{\text{L,PS}} = \rho\zeta l|h|^2 P. \tag{6}$$

The harvested energy assuming a nonlinear EH model [39] is given by

$$Q_{\text{NL,PS}} = \frac{P_s\left(1+e^{AB}\right)}{e^{AB}\left(1+e^{-A(\rho l|h|^2P-B)}\right)} - \frac{P_s}{e^{AB}}, \tag{7}$$

where P_s denotes the maximum harvested power when the energy harvesting circuit is saturated. Also, A and B are positive constants related to the circuit specification. Practically, A reflects the nonlinear charging rate with respect to the input power and B is related to (not exactly the same as) the turn-on threshold. Given the EH circuit, the parameters P_s, A, and B can be readily determined by the curve fitting.

2) Time-switching: Based on the same assumptions as in PS for the linear model, it follows that the harvested energy in the case of TS is given by

$$Q_{\text{L,TS}} = a\zeta l|h|^2 P. \tag{8}$$

Accordingly, for the nonlinear model the harvested energy is given by

$$Q_{\text{NL,TS}} = a\left(\frac{P_s\left(1+e^{AB}\right)}{e^{AB}\left(1+e^{-A(l|h|^2P-B)}\right)} - \frac{P_s}{e^{AB}}\right). \tag{9}$$

B. Achievable Rate

In what follows, the achievable rate for the considered PS and TS cases is derived.

Theorem 1. *The achievable rate of the considered setup assuming PS is expressed as*

$$R_{PS} = \frac{1}{2}\log_2\left(1+\frac{e(l|h|^2P)^2}{2\pi\sigma^2}\right) \tag{10}$$

with e representing Euler's number and

$$\sigma = \sigma^2_{rec} + \frac{\sigma^2_{ADC}}{(1-\rho)^2}. \tag{11}$$

Proof: The proof is provided in Appendix A. ■

In (10), the achievable rate depends on the PS factor only if the ADC noise is considered, which highlights its impact on the analysis.

Theorem 2. *The achievable rate of the considered setup assuming TS is expressed as*

$$R_{TS} = \frac{1}{2}(1-a)\log_2\left(1+\frac{e(l|h|^2P)^2}{2\pi(\sigma^2_{rec}+\sigma^2_{ADC})}\right). \tag{12}$$

Proof: The proof follows from Theorem 1. ■

It is noted that the above expressions differ from the Shannon capacity used in the separated receiver architecture, due to the square of the received power which once more highlights the importance of deriving the achievable rate in the integrated receiver architecture.

C. Harvested Energy−Data Rate Region

Capitalizing on the above two theorems and the equations of the harvested energy for both EH models, we determine the corresponding harvested energy−rate region for the considered setup. The achievable harvested energy−rate region for the point-to-point PS and TS system is illustrated in Fig. 3. To this effect, it can be observed that unlike the separated receiver architecture where PS always outperforms TS, in the considered integrated receiver architecture there is a region where the rate for the case of TS is greater than that for the case of PS, assuming equal harvested energies. This result can be proven by the following proposition for the case of the linear EH model.

Proposition 1. *Assuming that the amounts of harvested energy in the two techniques are equal and that the linear EH model is used, the achievable rate using TS is greater than the achievable rate using PS ($R_{TS} > R_{PS}$), when*

$$|h|^4 < \frac{2\pi a}{el^2P^2}\left(\frac{\sigma^2_{ADC}}{1-a} - \sigma^2_{rec}\right), \tag{13}$$

which is satisfied if $\sigma^2_{ADC}/(1-a) > \sigma^2_{rec}$.

Proof: The proof is provided in Appendix B. ∎

The above proposition insinuates that when utilizing the integrated receiver, PS is not always the best choice while the selection between PS and TS strategies relies, as expected, on the various system parameters.

Furthermore, for the PS case illustrated in Fig. 3, we can observe that even for the linear EH model, there is a region where the harvested energy−rate is concave and another one where it is convex. More specifically, the achievable rate in the case of the PS protocol and the linear EH model can be expressed as a function of the harvested energy as follows:

$$R(Q)=\frac{1}{2}\log_2\left(1+\frac{e(l|h|^2P)^2(\zeta l|h|^2P-Q)^2}{2\pi(\sigma_{\text{rec}}^2(\zeta l|h|^2P-Q)^2+\sigma_{\text{ADC}}^2(\zeta l|h|^2P)^2)}\right). \tag{14}$$

It is noted here that although the logarithm is a concave function, the term $(\zeta l|h|^2P-Q)^2$ causes the non-concavity of R with respect to Q.

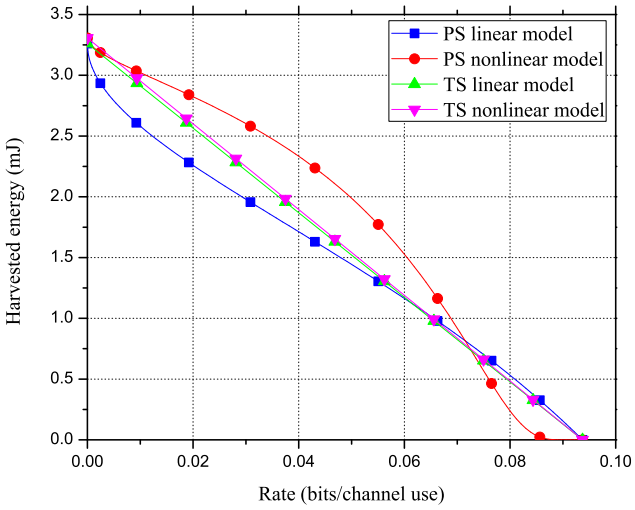

Fig. 3. Harvested energy−rate region with $P=2$W, $h\sim\mathcal{CN}(0,1)$, $\zeta=0.815$, $l=0.002$, $\frac{lP}{\sigma^2}=20$dB, $\sigma_{\text{rec}}^2=\sigma_{\text{ADC}}^2=\sigma^2$, $P_s=lP$, $A=6400$ and $B=0.003$.

IV. Joint Harvested Energy−Data Rate Outage Probability

Based on the derived results in Section III, the corresponding joint harvested energy−rate outage probability is derived.

A. Point-to-Point Communication with Power-splitting

The joint harvested energy−rate outage probability P_o is defined as the probability that the energy harvested by the user is lower than an energy threshold q_{th}, or the rate is lower than a rate threshold r_{th}. This definition can be expressed as

$$P_o=\Pr\left(Q\le q_{\text{th}}\cup R\le r_{\text{th}}\right), \tag{15}$$

where $\Pr(\cdot)$ denotes probability.

Theorem 3. *The joint harvested energy−rate outage probability for a point-to-point PS system is given by*

$$P_o=1-e^{-max\left\{v_1,\ \frac{1}{lP}\sqrt{\frac{2\pi\sigma^2}{e}\left(2^{2r_{th}}-1\right)}\right\}}, \tag{16}$$

where $max\{\cdot\}$ *denotes the maximum of the two elements and*

$$v_1=\begin{cases}\frac{q_{th}}{\rho\zeta lP}, & \textit{linear EH model},\\ \frac{1}{A\rho lP}\ln\left(\frac{q_{th}e^{AB}+P_s}{P_s-q_{th}}\right), & \textit{nonlinear EH model}.\end{cases} \tag{17}$$

Proof: The proof is provided in Appendix C. ∎

It is noted that in a SWIPT system, the aim is to minimize this probability. Hence, the optimal value of ρ is defined as

$$\rho^*=\arg\min_{\rho}P_o. \tag{18}$$

Proposition 2. *The optimal value of* $\rho\in[0,1]$ *is unique and is given by the solution of*

$$\rho^4-2\rho^3+\left(1+\frac{\sigma_{ADC}^2}{\sigma_{rec}^2}-\frac{c_1^2}{2\pi e\sigma_{rec}^2c_2^2}\right)\rho^2+\frac{2c_1^2}{\sigma_{rec}^2c_2^2}\rho-\frac{c_1^2}{\sigma_{rec}^2c_2^2}=0, \tag{19}$$

where

$$c_1=\begin{cases}\frac{q_{th}}{\zeta lP}, & \textit{linear EH model},\\ \frac{1}{AlP}\ln\left(\frac{q_{th}e^{AB}+P_s}{P_s-q_{th}}\right), & \textit{nonlinear EH model}\end{cases} \tag{20}$$

and

$$c_2=\frac{1}{lP}\sqrt{\frac{2\pi}{e}}\sqrt{2^{2r_{th}}-1}. \tag{21}$$

Proof: As the PS factor ρ increases, the first term in

$$\max\left\{v_1,\ \frac{1}{lP}\sqrt{\frac{2\pi\sigma^2}{e}\left(2^{2r_{\text{th}}}-1\right)}\right\}$$

decreases, while the second term increases. Thus, the probability is minimized when the above maximal value is minimized; that is, the two terms are equal and the optimal PS factor can be extracted from

$$\frac{c_1^2}{\rho^2}=\left(\sigma_{\text{rec}}^2+\frac{\sigma_{\text{ADC}}^2}{(1-\rho)^2}\right)c_2^2. \tag{22}$$

Assuming

$$f(\rho)=\frac{c_1^2}{\rho^2}-\left(\sigma_{\text{rec}}^2+\frac{\sigma_{\text{ADC}}^2}{(1-\rho)^2}\right)c_2^2, \tag{23}$$

it follows that $\lim_{\rho\to0}=\infty$ and $\lim_{\rho\to1}=-\infty$; thus there is at least one root of $f(\rho)$ in $[0,1]$. Moreover,

$$f'(\rho)=-\frac{2c_1^2}{\rho^3}-\frac{2c_2^2\sigma_{\text{ADC}}^2}{(1-\rho)^3}<0, \tag{24}$$

and thus f is a decreasing function in $[0,1]$ which implies that the above root is unique. To this effect and multiplying by $\rho^2(1-\rho)^2$ and dividing by $\sigma_{\text{rec}}^2c_2^2$, equation (22) can be rewritten as in (19). ∎

The closed-form expression for the optimal PS factor can be obtained by the general formulas for the roots of the quartic equation [47], [48]. Furthermore, the harvested energy threshold and the rate threshold region for a specific value of the joint harvested energy−rate outage probability can be represented as follows:

$$C_{q_{\text{th}},r_{\text{th}}}^{\text{PS}}=\bigcup_{\rho}\{(q_{\text{th}},r_{\text{th}}):q_{\text{th}}\le u_1,\ r_{\text{th}}\le \frac{1}{2}\log_2\left(1-\frac{\ln(1-P_o)e(lP)^2}{2\pi\sigma^2}\right),\ 0\le\rho\le1\}, \tag{25}$$

where

$$u_1=\begin{cases}-\ln(1-P_o)\rho\zeta lP, & \text{linear EH model,}\\ \frac{P_s\left(1+e^{AB}\right)}{e^{AB}\left(1+e^{A(\ln(1-P_o)\rho lP+B)}\right)}-\frac{P_s}{e^{AB}}, & \text{nonlinear EH model.}\end{cases} \tag{26}$$

Evidently, as q_{th} increases and the required probability remains the same, ρ needs to increase which leads to a reduction of r_{th}. Therefore, this causes a tradeoff between the two thresholds.

B. Point-to-Point Communication with Time-switching

This subsection provides the corresponding analytic results for the TS strategy.

Theorem 4. *The joint harvested energy−rate outage probability for a point-to-point TS system is given by*

$$P_o=1-e^{-max\left\{v_2,\ \frac{1}{lP}\sqrt{\frac{2\pi\left(\sigma_{rec}^2+\sigma_{ADC}^2\right)}{e}\left(2^{\frac{2r_{th}}{1-a}}-1\right)}\right\}}, \tag{27}$$

where

$$v_2=\begin{cases}\frac{q_{th}}{a\zeta lP}, & \textit{linear EH model},\\ \frac{1}{AlP}\ln\left(\frac{q_{th}e^{AB}+aP_s}{aP_s-q_{th}}\right), & \textit{nonlinear EH model}.\end{cases} \tag{28}$$

For the nonlinear model, the above expression holds when $a\in[\frac{q_{th}}{P_s},1]$. If $a\in[0,\frac{q_{th}}{P_s}]$, outage always occurs.

Proof: The proof follows from Theorem 3. ∎

Likewise, the optimal factor a is given in the following proposition.

Proposition 3. *The optimal TS factor $a\in[0,1]$ is unique and is given for the linear model by the solution of*

$$a^2\left(2^{\frac{2r_{th}}{1-a}}-1\right)-\frac{q_{th}^2e}{2\pi\zeta^2(\sigma_{rec}^2+\sigma_{ADC}^2)}=0, \tag{29}$$

and for the nonlinear model by the solution of

$$\left(2^{\frac{2r_{th}}{1-a}}-1\right)\ln^{-2}\left(\frac{aP_s-q_{th}}{q_{th}e^{AB}+aP_s}\right)-\frac{e}{2\pi A^2(\sigma_{rec}^2+\sigma_{ADC}^2)}=0. \tag{30}$$

Proof: The proof follows from Proposition 2. ∎

Moreover, the harvested energy threshold and the rate threshold region for a specific value of the joint harvested energy−rate outage probability can be described as follows:

$$C_{q_{\text{th}},r_{\text{th}}}^{\text{TS}}=\bigcup_a\Bigg\{(q_{\text{th}},r_{\text{th}}):q_{\text{th}}\le u_2,\ r_{\text{th}}\le\frac{1}{2}(1-a)\times\log_2\left(1-\frac{\ln(1-P_o)e(lP)^2}{2\pi(\sigma_{\text{rec}}^2+\sigma_{\text{ADC}}^2)}\right),0\le a\le1\Bigg\}, \tag{31}$$

where

$$u_2=\begin{cases}-\ln(1-P_o)a\zeta lP, & \text{linear EH model,}\\ a\left(\frac{P_s\left(1+e^{AB}\right)}{e^{AB}\left(1+e^{A(\ln(1-P_o)lP+B)}\right)}-\frac{P_s}{e^{AB}}\right), & \text{nonlinear model.}\end{cases} \tag{32}$$

C. Downlink Multicasting with Power-splitting

In a downlink multicasting PS system, the harvested energy by the n-th user for the linear EH model is given by

$$Q_{\text{L,PS,n}}=\rho_n\zeta_nl_n|h_n|^2P, \tag{33}$$

and for the nonlinear EH model by

$$Q_{\text{NL,PS,n}}=\frac{P_s\left(1+e^{AB}\right)}{e^{AB}\left(1+e^{-A(\rho_nl_n|h|^2P-B)}\right)}-\frac{P_s}{e^{AB}}. \tag{34}$$

With the aid of (10), the achievable rate of the n-th user is given by

$$R_{\text{PS,n}}=\frac{1}{2}\log_2\left(1+\frac{e(l_n|h_n|^2P)^2}{2\pi\sigma_n^2}\right). \tag{35}$$

Theorem 5. *The joint harvested energy−rate outage probability for a multicasting PS system, which is defined as the probability that at least one user is in outage, is given by*

$$P_o=1-\prod_{n=1}^{N}e^{-max\left\{v_3,\ \frac{1}{l_nP}\sqrt{\frac{2\pi\sigma_n^2}{e}\left(2^{2r_{th}}-1\right)}\right\}}, \tag{36}$$

where

$$v_3=\begin{cases}\frac{q_{th,n}}{\rho_n\zeta_nl_nP}, & \textit{linear EH model},\\ \frac{1}{A\rho_nl_nP}\ln\left(\frac{q_{th,n}e^{AB}+P_s}{P_s-q_{th,n}}\right), & \textit{nonlinear EH model}.\end{cases} \tag{37}$$

Proof: The joint harvested energy−rate outage probability can be expressed as

$$P_o=\Pr\left(Q_1\le q_{\text{th,1}}\cup R_1\le r_{\text{th}}\cup\cdots\cup Q_N\le q_{\text{th,N}}\cup R_N\le r_{\text{th}}\right). \tag{38}$$

It is noted here that the energy threshold can be practically different in each user; however, the same does not hold for the rate, due to the multicasting principle. Hence, exploiting the complementary event and since $|h_n|^2$ are statistically independent for all values of $n\in\{1,...,N\}$, equation (38) can be expressed as

$$P_o=1-\prod_{n=1}^{N}\Pr\left(Q_n\le q_{\text{th,n}}\cup R_n\le r_{\text{th}}\right). \tag{39}$$

Therefore, the joint harvested energy−rate outage probability for a multicasting PS system is obtained by (36), which completes the proof. ∎

It is noted that the optimal PS factor for each user in Theorem 5 can be determined following Proposition 2.

D. Downlink Multicasting with Time-switching

In the case of multicasting TS system and recalling (8), the harvested energy by the n-th user for the linear EH model is given by

$$Q_{\text{L,TS,n}}=a_n\zeta_nl_n|h_n|^2P, \tag{40}$$

whereas for the nonlinear EH model it is given by

$$Q_{\text{NL,TS,n}}=a_n\left(\frac{P_s\left(1+e^{AB}\right)}{e^{AB}\left(1+e^{-A(l_n|h|^2P-B)}\right)}-\frac{P_s}{e^{AB}}\right). \tag{41}$$

Accordingly, from (12), the achievable rate of the n-th user is expressed as

$$R_{\text{TS,n}} = \frac{1}{2}(1-a_n)\log_2\left(1+\frac{e(l_n|h_n|^2P)^2}{2\pi\left(\sigma^2_{\text{rec,n}}+\sigma^2_{\text{ADC,n}}\right)}\right). \quad (42)$$

Theorem 6. *The joint harvested energy−rate outage probability for a multicasting TS system is given by*

$$P_o = 1-\prod_{n=1}^{N} e^{-max\left\{v_4,\ \frac{1}{l_nP}\sqrt{\frac{2\pi\left(\sigma^2_{rec,n}+\sigma^2_{ADC,n}\right)}{e}\left(2^{\frac{2r_{th}}{1-a_n}}-1\right)}\right\}}, \quad (43)$$

where

$$v_4 = \begin{cases} \frac{q_{th,n}}{a_n\zeta_n l_n P}, & \textit{linear EH model},\\ \frac{1}{Al_nP}\ln\left(\frac{q_{th,n}e^{AB}+aP_s}{aP_s-q_{th,n}}\right), & \textit{nonlinear EH model}. \end{cases} \quad (44)$$

Proof: The proof is derived using (40), (41) and (42), and following the methodology of the proof of Theorem 5. ∎

The optimal TS factor for each user can be determined with the aid of Proposition 3.

V. Dynamic Resource Allocation in Downlink Broadcasting

In this section, a downlink broadcasting system is considered which consists of one BS and N users. With the aim to emphasize on the impact of the provided expressions of the capacity on the investigation of performance of the integrated receiver, we focused on a subset of all possible assumptions. In this context, let T_{tot} denote the block transmission time, which is measured in seconds. Also, τ_n (unitless value) is the portion of time in which information transmission is enabled for the n-th user, with $\sum_{n=1}^{N}\tau_n = 1$, according to the principles of time division multiple access (TDMA). During this time interval, all other users utilize the transmitted power for EH. Without loss of generality, it is henceforth assumed that $T_{\text{tot}} = 1$ sec. Therefore, the interval of allocated time in the n-th user is τ_n in seconds. In the considered optimization problem, both the allocated time and the transmit power in each time slot are subject to optimization and, thus, ignoring the ADC noise might lead to an impractical received SNR for some time intervals. In order to avoid further increase of complexity, we assume that PS is not utilized, i.e., a user performs EH solely during the time intervals in which information transmission is enabled for any of the other users. Also, the linear EH model is assumed. In this context, the alternation between the EH and ID is enabled by the TS strategy.

Based on the above, the harvested energy by the n-th user is given by

$$Q_n = \zeta_n l_n |h_n|^2 \sum_{m\neq n}\tau_m P_m. \quad (45)$$

Accordingly, the n-th user decodes information for time τ_n and from (12), the achievable rate is given by

$$R_n = \frac{1}{2}\tau_n\log_2\left(1+\frac{e(l_n|h_n|^2P_n)^2}{2\pi\left(\sigma^2_{\text{rec,n}}+\sigma^2_{\text{ADC,n}}\right)}\right). \quad (46)$$

The aim in this system is to maximize the total harvested energy Q_t, which is the sum of the energy harvested by each user, while the information rate of each user remains greater than a predetermined threshold. To this end, this optimization problem can be formulated as follows:

$$\begin{aligned} \underset{\tau,\mathcal{P}}{\textbf{max}}\quad & Q_t \\ \textbf{s.t.}\quad & \mathrm{C}_1:\ R_n \geq r_{\text{th,n}},\ \forall n,\\ & \mathrm{C}_2:\ \textstyle\sum_{n=1}^{N}\tau_n P_n \leq P_t,\\ & \mathrm{C}_3:\ \textstyle\sum_{n=1}^{N}\tau_n \leq 1,\\ & \mathrm{C}_4:\ P_n \geq 0,\ \forall n,\\ & \mathrm{C}_5:\ \tau_n \geq 0,\ \forall n, \end{aligned} \quad (47)$$

where $\tau = \{0 \leq \tau_n \leq 1, \forall n\}$ and $\mathcal{P} = \{P_n \geq 0, \forall n\}$, whereas P_t denotes the total transmit power and $r_{\text{th,n}}$ denotes the rate threshold. Notably, with the aid of (45) and (46), the above problem can be rewritten as

$$\begin{aligned} \underset{\tau,\mathcal{P}}{\textbf{max}}\quad & \textstyle\sum_{n=1}^{N}\zeta_n l_n|h_n|^2\sum_{m\neq n}\tau_m P_m \\ \textbf{s.t.}\quad & \mathrm{C}_1:\ \tfrac{1}{2}\tau_n\log_2\left(1+\frac{e(l_n|h_n|^2P_n)^2}{2\pi\left(\sigma^2_{\text{rec,n}}+\sigma^2_{\text{ADC,n}}\right)}\right)\geq r_{\text{th,n}},\ \forall n,\\ & \mathrm{C}_2:\ \textstyle\sum_{n=1}^{N}\tau_n P_n \leq P_t,\\ & \mathrm{C}_3:\ \textstyle\sum_{n=1}^{N}\tau_n \leq 1,\\ & \mathrm{C}_4:\ P_n \geq 0,\ \forall n,\\ & \mathrm{C}_5:\ \tau_n \geq 0,\ \forall n. \end{aligned} \quad (48)$$

It is evident that the sum of the transmit energy regarding each user must be lower than or equal to the total transmit energy (C_2). Likewise, C_4 indicates that the average transmit power regarding the n-th user must be a non-negative number, whereas τ_n denotes time interval and, thus, it is a non-negative value (C_5). It is also noted here that the achievable rate and the harvested energy for the n-th and m-th users, $\forall m \neq n$, respectively, are both increasing functions of τ_n and P_n, for fixed τ_m and P_m, $\forall m \neq n$. Based on this, the inequality in C_2 can be replaced by equality, without excluding the optimal from the set of all solutions. To this effect, equation (48) can be rewritten as follows:

$$\begin{aligned} \underset{\tau,\mathcal{P}}{\textbf{max}}\quad & \textstyle\sum_{n=1}^{N}\zeta_n l_n|h_n|^2(P_t-\tau_n P_n) \\ \textbf{s.t.}\quad & \mathrm{C}_1,\mathrm{C}_2,\mathrm{C}_3,\mathrm{C}_4,\mathrm{C}_5. \end{aligned} \quad (49)$$

Importantly, the above optimization problem is non-convex because of both the objective function and the first constraint. The non-convexity in combination with the fact than the problem is high dimensional with multiple variables results in a high computational cost required to calculate the global optimal solution. To this end, by setting $\tau_n \triangleq \exp(\tilde{\tau}_n)$ and $P_n \triangleq \exp(\tilde{P}_n)$, equation (49) can be rewritten as

$$\begin{aligned} \underset{\tilde{\tau},\tilde{\mathcal{P}}}{\textbf{max}}\quad & \textstyle\sum_{n=1}^{N}\zeta_n l_n|h_n|^2(P_t-\exp(\tilde{\tau}_n+\tilde{P}_n)) \\ \textbf{s.t.}\quad & \mathrm{C}_1:\ \tfrac{1}{2}\exp(\tilde{\tau}_n)\log_2\left(1+\frac{el_n^2|h_n|^4\exp(2\tilde{P}_n)}{2\pi\left(\sigma^2_{\text{rec,n}}+\sigma^2_{\text{ADC,n}}\right)}\right)\geq r_{\text{th,n}},\forall n,\\ & \mathrm{C}_2:\ \textstyle\sum_{n=1}^{N}\exp(\tilde{\tau}_n+\tilde{P}_n) \leq P_t,\\ & \mathrm{C}_3:\ \textstyle\sum_{n=1}^{N}\exp(\tilde{\tau}_n) \leq 1,\\ & \mathrm{C}_4:\ \exp(\tilde{P}_n)\geq 0,\ \forall n,\\ & \mathrm{C}_5:\ \exp(\tilde{\tau}_n)\geq 0,\ \forall n, \end{aligned} \quad (50)$$

where $\tilde{\tau} = \{\tilde{\tau}_n, \forall n\}$ and $\tilde{\mathcal{P}} = \{\tilde{P}_n, \forall n\}$. In (49), C_4 and C_5 can be omitted, as they are satisfied for every value of $\tilde{\mathcal{P}}$ and $\tilde{\tau}$, respectively. Furthermore, C_1 can be rewritten as follows:

$$1 + \frac{el_n^2|h_n|^4}{2\pi\left(\sigma_{\text{rec,n}}^2 + \sigma_{\text{ADC,n}}^2\right)} \exp(2\tilde{P}_n) \geq 2^{2r_{\text{th,n}}\exp(-\tilde{\tau}_n)} \quad (51)$$

which after some mathematical manipulations yields

$$\ln\left(2^{2r_{\text{th,n}}\exp(-\tilde{\tau}_n)} - 1\right) - \ln\frac{el_n^2|h_n|^4}{2\pi\left(\sigma_{\text{rec,n}}^2 + \sigma_{\text{ADC,n}}^2\right)} - 2\tilde{P}_n \leq 0. \quad (52)$$

Based on this and with the aid of (52), equation (49) can be rewritten as

$$\begin{aligned} \max_{\tilde{\tau},\tilde{\mathcal{P}}} \quad & \textstyle\sum_{n=1}^{N} \zeta_n l_n |h_n|^2 (P_t - \exp(\tilde{\tau}_n + \tilde{P}_n)) \\ \text{s.t.} \quad & C_1 : \ln\left(2^{2r_{\text{th,n}}\exp(-\tilde{\tau}_n)} - 1\right) - 2\tilde{P}_n \leq \ln\frac{el_n^2|h_n|^4}{2\pi\left(\sigma_{\text{rec,n}}^2+\sigma_{\text{ADC,n}}^2\right)}, \forall n, \\ & C_2 : \textstyle\sum_{n=1}^{N} \exp(\tilde{\tau}_n + \tilde{P}_n) \leq P_t, \\ & C_3 : \textstyle\sum_{n=1}^{N} \exp(\tilde{\tau}_n) \leq 1. \end{aligned} \quad (53)$$

Lemma 1. *The optimization problem described in* (53) *is convex.*

Proof: The proof is provided in Appendix D. ∎

Lemma 1 is critical in that it simplifies significantly the optimization problem and thus, rendering it solvable. To this end, having proven the convexity of the optimization problem, the following proposition can be used to derive the optimal solutions of (47).

Proposition 4. *Let λ_n, μ, and ν be the Lagrange multipliers (LMs) that correspond to the constraints C_1, C_2, and C_3, respectively, of* (53)*. Then, the global optimal power and time allocation can be respectively expressed as*

$$P_n^* = \frac{2\lambda_n}{\tau_n^*(\mu + \zeta_n l_n |h_n|^2)} \quad (54)$$

and

$$\tau_n^* = \frac{z_n}{2r_{\text{n}}}, \quad (55)$$

where z_n is given by

$$\frac{\lambda_n \ln 2}{2r_{th,n}} 2^{z_n} z_n^2 = \left(\nu + \frac{\lambda_n}{r_{th,n}} z_n\right)(2^{z_n} - 1). \quad (56)$$

Proof: The proof is provided in Appendix E. ∎

Proposition 4 highlights the physical interpretation of the derived solution as well as that several calculations can be performed in parallel.

VI. Simulation Results and Discussion

In this section, we use the obtained analytical and simulation results to quantify the performance and the characteristics of the proposed contribution. The path loss factor is given by [39], i.e., $l = 1 - e^{-\frac{a_t a_r}{(c/f)^2 d^2}}$, where a_t is the aperture of the transmit antenna, a_r the aperture of the receive antenna, c the velocity of light, f_c the operating frequency and d the distance between the transmitter and the receiver. Assuming the receiver as a small sensor, we set $a_t = 0.5$m, $a_r = 0.01$m and $f_c = 2.4$GHz. Moreover, without loss of generality and unless stated otherwise, it is assumed that $P = 2$W, $lP/\sigma^2 = 20$dB, $\sigma_{\text{rec}}^2 = \sigma_{\text{ADC}}^2 = \sigma^2$ and $\zeta = 0.815$ [39], whereas the distance for all users is considered $d = 12$m. Regarding the nonlinear EH model, it is considered that $P_s = lP$, $A = 6400$ and $B = 0.003$. Also, in all figures, the values of ρ and a are optimally selected.

In Fig. 4, a point-to-point system, a multicasting system of two users and a multicasting system of three users are demonstrated for the cases of PS and TS when the nonlinear EH model is used. The harvested energy threshold is set to $q_{\text{th}} = 1$mJ and the rate threshold to $r_{\text{th}} = 0.01$ bits/channel use. The joint harvested energy−rate outage probabilities of the three systems are compared, when the distance of the users increases. As it can be observed, in long distances the number of users has limited effect on the overall performance. Also, it is evident that TS outperforms PS for all systems with the considered setup.

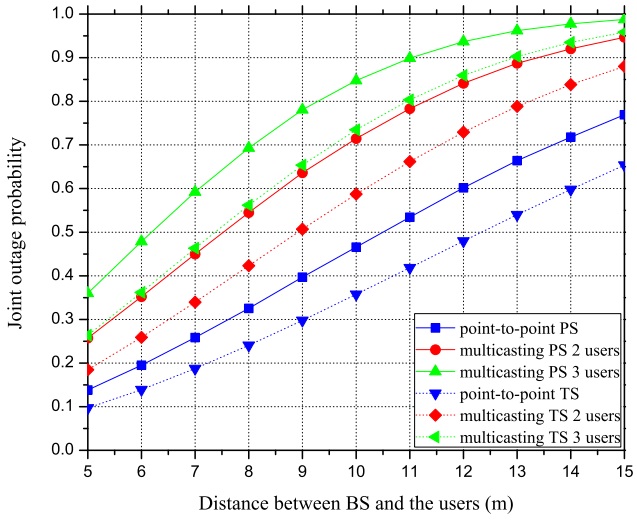

Fig. 4. Outage probability versus distance d.

Likewise, in Fig. 5, the joint harvested energy−rate outage probability of the same systems is plotted against the transmit power when the nonlinear EH model is used, with $q_{\text{th}} = 1$mJ and $r_{\text{th}} = 0.01$ bits/channel use. It is evident that the performance of point-to-point systems for both PS and TS clearly outperform the performance of the multicasting counterparts for two and three users, whereas TS still outperforms the PS counterpart. The improved performance of the TS protocol compared to the PS counterpart remains the same as the transmit power increases. However, it is evident that the corresponding performance improvement exhibits saturation in terms of increasing transmit power. As a result, it can be concluded that the selection of the protocol, i.e., PS or TS, based on the system parameters is crucial since it is not practically effective to assume that such performance compensations can be achieved by simply increasing the transmit power.

Figs. 6 and 7 illustrate the effect of both thresholds for harvested energy and achievable rate on the joint outage probability and the optimal selection of ρ. It is evident that as the thresholds increase, the joint outage probability also increases, whereas the optimal PS factor increases when the energy threshold increases or the rate threshold decreases. Also, it

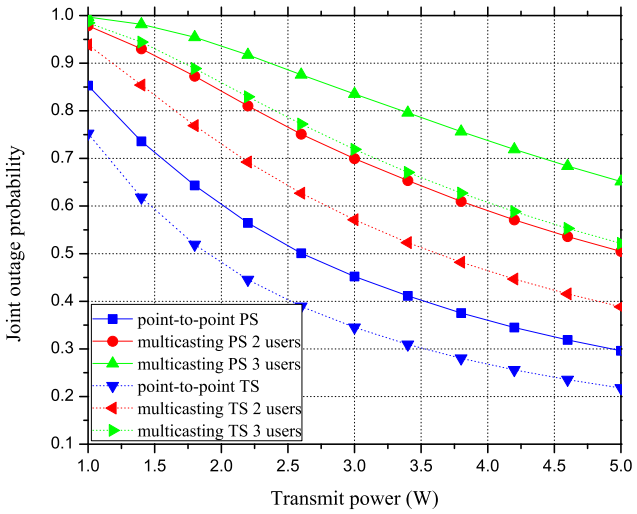

Fig. 5. Outage probability versus transmit power.

is observed that $\rho^* \in [0, 1]$ spans a large range of values for different thresholds. This is an interesting observation and highlights the importance of the ADC noise, since when this is ignored, the achievable rate is independent of the PS factor and, thus, $\rho^* \to 1$ [41]. In this case a small portion of the signal is used for ID and, thus, the ADC becomes comparable to the signal power and with a potentially destructive impact to the achievable quality of communication. Likewise, a similar trend is observed for the case of the considered multicasting system, the performance of which is illustrated in Fig. 8, for two users and $d_n = 12$m, $n \in \{1, 2\}$. It is noted here that such figures have not been included for TS and the linear EH model, because they are rather similar to the ones presented for the case of PS.

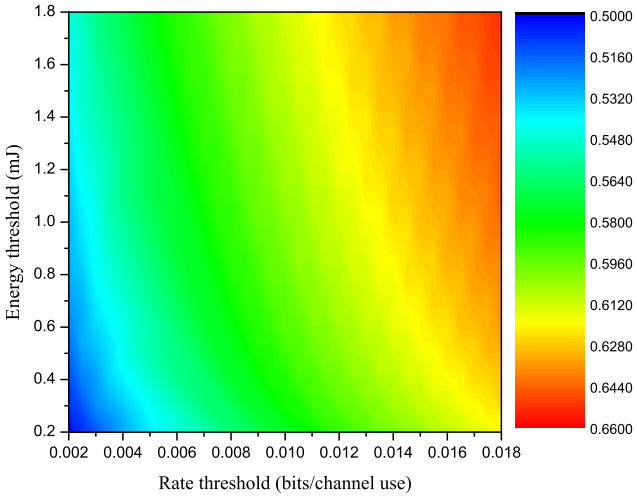

Fig. 6. Outage probability versus energy and rate thresholds in a point-to-point PS system.

Figs. 9, 10, and 11 illustrate the results of the dynamic resource allocation in the downlink broadcasting system. In this case, when a specific optimization problem is not feasible, due to the values of the channel gain, the harvested energy is considered equal to zero. The average harvested energy per user, which is computed as the total energy harvested by all

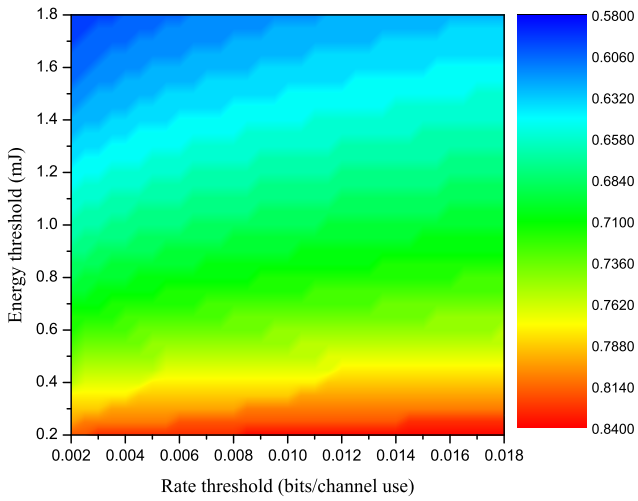

Fig. 7. Optimal PS factor versus energy and rate thresholds in a point-to-point PS system.

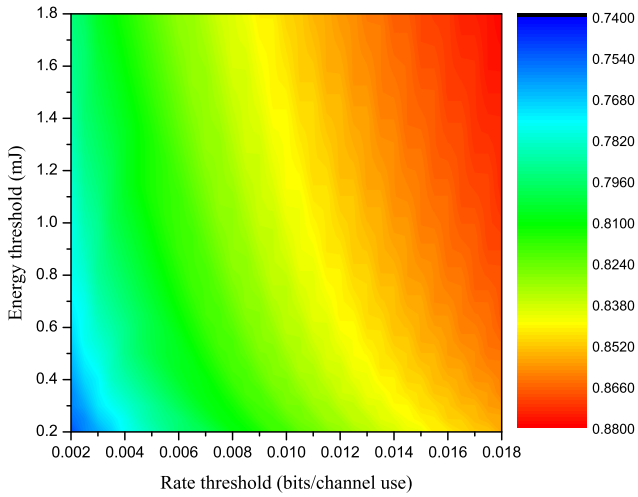

Fig. 8. Outage probability versus energy and rate thresholds in a multicasting PS system.

users divided by the number of users, is considered as the appropriate metric to ensure a fair comparison of systems that consist of a different number of users.

In Fig. 9, a downlink broadcasting system consisting of two users is simulated. When any of the rate thresholds increases, the transmitted power used to achieve the desired rate and, thus, the average harvested energy per user decreases. Furthermore, the average harvested energy per user is particularly sensitive to the distance of the users from the BS, as the harvested energy decreases rapidly when moving a user away from the BS. However, this decrease occurs at a lower rate, as the users are further away from the BS. A case of special interest is when the two users have the same total required rate, but asymmetrical rate requirements, which corresponds to the curves with $r_{\mathrm{th},1} = 0.015, r_{\mathrm{th},2} = 0.01$ and $r_{\mathrm{th},1} = 0.01, r_{\mathrm{th},2} = 0.015$. When the nearest user to the BS has a higher QoS requirement, this is achieved with less resources, and therefore the average harvested energy increases. In fact, it is observed that the effect of this is more profound at higher distances, where the difference between the

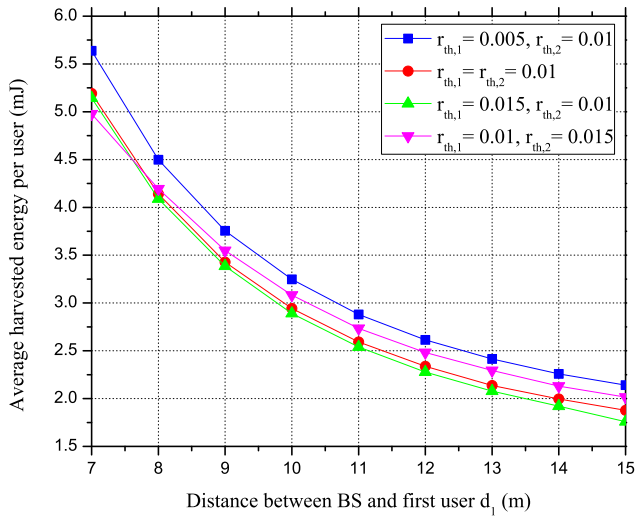

Fig. 9. Average harvested energy per user versus distance d_1.

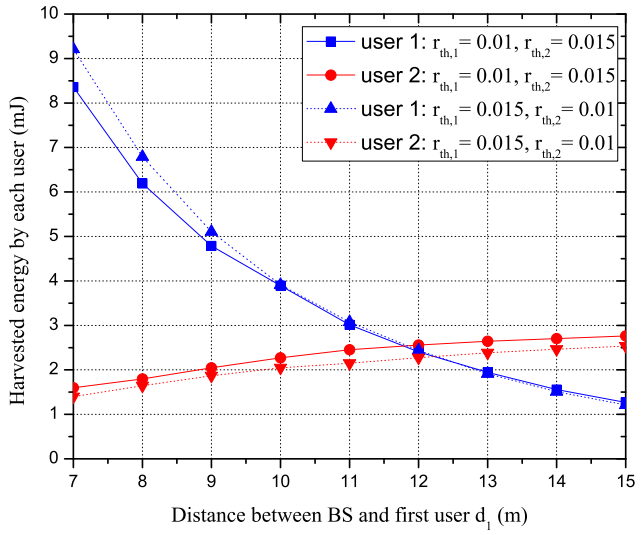

Fig. 10. Harvested energy by each of two users versus distance d_1.

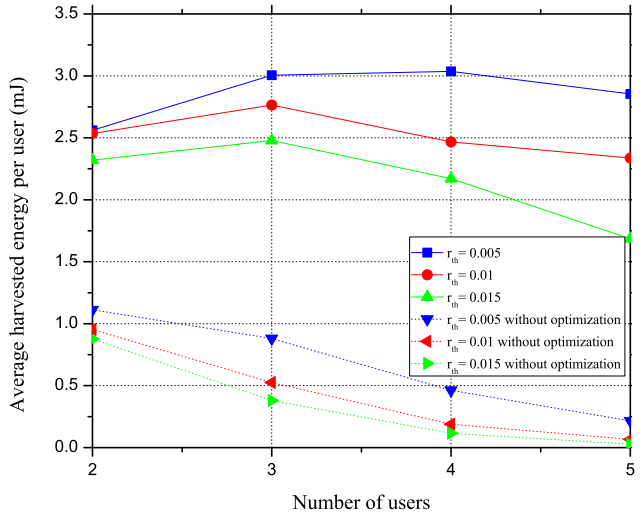

Fig. 11. Average harvested energy per user versus number of users.

demonstrated scenarios is greater.

In Fig. 10, the energy harvested by each one of the two users is plotted against the distance of the first user for two different pairs of rate thresholds. It can be observed that when the distance of the first user is lower than that of the second user, the energy harvested by the first user is higher. Also, when the rate threshold of a specific user is higher compared to the threshold of the other user, this user harvests less energy. Also, in the case of long distances, the harvested energy by the first user coincides for the different rate thresholds.

Finally, in Fig. 11, the average harvested energy per user is presented in broadcasting systems consisting of different number of users, when all users have the same rate threshold and are located at the same distance of 12m. In this context, the performance of the proposed optimization is compared against the case that power and time are equally allocated among the users. It is evident that the proposed method leads to remarkable gains for all the rate thresholds, despite the number of users. When $r_{\text{th}} = 0.015$ bits/channel use, as the number of users increases to four or five users the performance drops; this is because the rate constraint is more rarely satisfied for all users and, thus, for many channels realizations the optimization problem is not feasible. It is notable that when $r_{\text{th}} = 0.01$ bits/channel use, the system consisting of three users performs better than other setups with a different number of users. On the contrary, when the rate threshold is reduced to 0.005 bits/channel use, the systems of three, four, and five users exhibit similar performance with respect to the average harvested energy per user. Furthermore, a non-monotonicity is observed which is because more users can harvest energy during time intervals with relatively high amounts of transmitted energy ($P_n\tau_n$) as the number of users increases, while, on the other hand, all users need to achieve the achievable rate threshold. These two phenomena have a conflicting impact on the average harvested energy per user. It is recalled that if the problem is infeasible, i.e., if C_1 cannot be satisfied for all users, it is assumed that the harvested energy at this specific time slot is zero, in order to justify the corresponding degradation to performance due to the increase of the number of users. This also justifies that the maximum performance (i.e., the extremum of the harvested energy per user) is achieved for a lower number of users as the rate threshold increases.

VII. Conclusions

This work has investigated the performance of the integrated energy and information receiver. The tradeoff between the harvested energy and the achievable rate has been quantified when PS and TS strategies are assumed, both for a linear and a nonlinear EH model. To this end, the achievable harvested energy−rate region and the theoretical analysis has shown that there is a region where TS outperforms PS, unlike the trend in common separated receivers. To balance the tradeoff between the harvested energy and the rate in a point-to-point and in a multicasting system, the joint harvested energy−rate outage probability has been introduced and minimized. Also, the ADC noise has been considered, which has a critical impact on the optimal selection of the PS and the TS factor. Furthermore, a

dynamic resource allocation has been achieved in a TS-based broadcasting system, aiming to maximize the total energy harvested by all users while maintaining the achievable rate above a specific threshold. The derived results have shown that this receiver can be used in systems consisting of many users in the absence of requirement for high rates.

The proposed theoretical framework in the considered analysis facilitates the investigation of the performance of the integrated receiver, which is fundamentally different to the separated receiver and creates opportunities for future research on this topic. Also, the results obtained with the assumptions in this paper can be viewed as the benchmark for the evaluation of the performance of other schemes. For example, the advantages of this receiver regarding the complexity and the power consumption can lead to the utilization of this receiver in multiple antennas scenarios. Furthermore, the performance of this receiver architecture can be examined without the assumption of perfect CSI. Finally, the effect of the input distribution on the harvested energy can be investigated in the integrated receiver architecture.

Appendix A
Proof of Theorem 1

The channel capacity relates to the mutual information between the input and the output of the channel through the inequality

$$C \geq I(X,Y), \tag{57}$$

where the equality holds for the optimal input distribution. From (57), a capacity lower bound can be obtained, using a random input distribution subject to $X \in \mathbb{R}^+$ and $\mathbb{E}[X] \leq 1$.

The mutual information between the input and the output of the channel (3) can be written as

$$\begin{aligned} I(X,Y) &= H(Y) - H(Y|X) && (58)\\ &= H(l|h|^2PX + Z) - H(Z) && (59)\\ &= \frac{1}{2}\log_2\left(2^{2H(l|h|^2PX+Z)}\right) - H(Z), && (60)\end{aligned}$$

where $H(\cdot)$ denotes the corresponding information entropy. For the first term in (60), it holds that [49]

$$\frac{1}{2}\log_2\left(2^{2H(l|h|^2PX+Z)}\right) \geq \frac{1}{2}\log_2\left(2^{2H(l|h|^2PX)} + 2^{2H(Z)}\right). \tag{61}$$

As a result, equation (60) can be rewritten as

$$I(X,Y) \geq \frac{1}{2}\log_2\left(1 + \frac{2^{2H(l|h|^2PX)}}{2^{2H(Z)}}\right). \tag{62}$$

Considering that Z follows the normal distribution, the entropy of the equivalent processing noise is expressed as

$$H(Z) = \frac{1}{2}\log_2\left(2\pi e\sigma^2\right). \tag{63}$$

With the aid of (63), equation (62) can be rewritten as

$$I(X,Y) \geq \frac{1}{2}\log_2\left(1 + \frac{2^{2H(l|h|^2PX)}}{2\pi e\sigma^2}\right), \tag{64}$$

where the exponent in the numerator in (64) can be rewritten as [49]

$$\begin{aligned} H(l|h|^2PX) &= H(X) + \log_2(|l|h|^2P|) && (65)\\ &= H(X) + \log_2(l|h|^2P), && (66)\end{aligned}$$

where l, $|h|^2$ and P are positive constants.

The channel in (3) is known as optical intensity channel [50]. It has been shown that for this channel a tight capacity lower bound is obtained by mutual information when the input X follows exponential distribution. The rate parameter of the exponential distribution is set to unity in order to maximize the derived achievable rate and for the restriction $\mathbb{E}[X] \leq 1$ to be satisfied. The entropy of X under this distribution is

$$H(X) = \frac{1}{\ln 2}. \tag{67}$$

From (64), the mutual information is computed, assuming that the input distribution is exponential. Using the equality, the capacity lower bound is obtained, which is considered as the achievable rate and is given by

$$R_{\text{PS}} = \frac{1}{2}\log_2\left(1 + \frac{2^{2(\frac{1}{\ln 2} + \log_2(l|h|^2P))}}{2\pi e\sigma^2}\right). \tag{68}$$

Based on this, equation (10) is deduced, which completes the proof.

Appendix B
Proof of Proposition 1

When $Q_{\text{PS}} = Q_{\text{TS}}$, it follows from (6) and (8) that $\rho = a$. To this effect and setting

$$A = \frac{e(l|h|^2P)^2}{2\pi}, \tag{69}$$

the comparison of (12) and (10) can be represented as

$$(1-a)\ln\left(1 + \frac{A}{\sigma^2_{\text{rec}} + \sigma^2_{\text{ADC}}}\right) > \ln\left(1 + \frac{A}{\sigma^2_{\text{rec}} + \frac{\sigma^2_{\text{ADC}}}{(1-a)^2}}\right). \tag{70}$$

By recalling that

$$\frac{x-1}{x} \leq \ln x \leq x - 1, \qquad \forall x > 0, \tag{71}$$

for the first part of (70), it follows that

$$(1-a)\ln\left(1 + \frac{A}{\sigma^2_{\text{rec}} + \sigma^2_{\text{ADC}}}\right) \geq (1-a)\frac{A}{\sigma^2_{\text{rec}} + \sigma^2_{\text{ADC}} + A}, \tag{72}$$

whereas for the second part of (70), one obtains

$$\frac{A}{\sigma^2_{\text{rec}} + \frac{\sigma^2_{\text{ADC}}}{(1-a)^2}} \geq \ln\left(1 + \frac{A}{\sigma^2_{\text{rec}} + \frac{\sigma^2_{\text{ADC}}}{(1-a)^2}}\right). \tag{73}$$

Considering (72) and (73), equation (70) is valid if

$$(1-a)\frac{A}{\sigma^2_{\text{rec}} + \sigma^2_{\text{ADC}} + A} > \frac{A}{\sigma^2_{\text{rec}} + \frac{\sigma^2_{\text{ADC}}}{(1-a)^2}}, \tag{74}$$

which yields (13) and, thus, completes the proof.

APPENDIX C
PROOF OF THEOREM 3

The proof refers to the linear EH model, as the one for the nonlinear model is similar. With the aid of (6) and (10), equation (15) can be rewritten as

$$P_o = \Pr\left(\rho\zeta l|h|^2 P \leq q_{\text{th}} \cup \frac{1}{2}\log_2\left(1+\frac{e(l|h|^2P)^2}{2\pi\sigma^2}\right) \leq r_{\text{th}}\right) \tag{75}$$

where by recalling that the random variable of both events is $|h|^2$ becomes

$$P_o = \Pr\left(|h|^2 \leq \frac{q_{\text{th}}}{\rho\zeta lP} \cup |h|^2 \leq \frac{1}{lP}\sqrt{\frac{2\pi\sigma^2}{e}\left(2^{2r_{\text{th}}}-1\right)}\right). \tag{76}$$

It can be observed that the random variable $|h|^2$ is upper bounded in both events. The union of these events occurs when $|h|^2$ is lower than the maximum of these upper bounds. Hence, P_o can be expressed as

$$P_o = \Pr\left(|h|^2 \leq \max\left\{\frac{q_{\text{th}}}{\rho\zeta lP},\ \frac{1}{lP}\sqrt{\frac{2\pi\sigma^2}{e}\left(2^{2r_{\text{th}}}-1\right)}\right\}\right). \tag{77}$$

It is recalled that $h \sim \mathcal{CN}(0,1)$; consequently, $|h|$ follows a Rayleigh distribution with scale parameter $1/\sqrt{2}$, whereas $|h|^2$ follows an exponential distribution with rate parameter 1. The probability density function for this distribution is $f(x) = e^{-x}$ and the outage probability is given by

$$P_o = \int_0^{\max\left\{\frac{q_{\text{th}}}{\rho\zeta lP},\ \frac{1}{lP}\sqrt{\frac{2\pi\sigma^2}{e}\left(2^{2r_{\text{th}}}-1\right)}\right\}} e^{-x}dx. \tag{78}$$

Based on the above and after some algebraic manipulations, equation (16) is deduced, which completes the proof.

APPENDIX D
PROOF OF LEMMA 1

The second term in the objective function is sum-exp functions and, thus, convex. As a result, the objective function is concave. Also, the left side of the constraints C_2 and C_3 are sum-exp functions and, thus, convex. Regarding C_1, setting the first term as $f(\tilde{\tau}_n)$, the second derivative is given by

$$\begin{aligned}\frac{d^2f}{d\tilde{\tau}_n^2} =& 2\ln 2\frac{2^{2r_{\text{th,n}}\exp(-\tilde{\tau}_n)}r_{\text{th,n}}\exp(-\tilde{\tau}_n)}{(2^{2r_{\text{th,n}}\exp(-\tilde{\tau}_n)}-1)^2}\\ &\times\left((2^{2r_{\text{th,n}}\exp(-\tilde{\tau}_n)}-1)\exp(\tilde{\tau}_n)-2r_{\text{th,n}}\ln 2\right),\end{aligned} \tag{79}$$

where it must be proven that $d^2f/d\tilde{\tau}_n^2 \geq 0$ or

$$(2^{2r_{\text{th,n}}\exp(-\tilde{\tau}_n)}-1)\frac{\exp(\tilde{\tau}_n)}{2r_{\text{th,n}}\ln 2}-1 \geq 0. \tag{80}$$

To this effect, setting

$$x = 2r_{\text{th,n}}\exp(-\tilde{\tau}_n) \tag{81}$$

and

$$g(x) = \frac{2^x-1}{x\ln 2}-1 = \frac{2^x - x\ln 2 - 1}{x\ln 2}, \tag{82}$$

the derivative of the numerator in (82) is expressed as

$$\frac{d(2^x - x\ln 2 - 1)}{dx} = (2^x-1)\ln 2, \tag{83}$$

which is positive, as $x > 0$, and $\lim_{x\to 0}(2^x - x\ln 2 - 1) = 0$. Thus, $g(x)$ is positive, from which, equation (80) is derived. In C_1, the second term is linear and it does not affect the concavity. Thus, the proof is complete.

APPENDIX E
PROOF OF PROPOSITION 4

The Lagrangian of (53) is given by

$$\begin{aligned}\mathcal{L} =& \sum_{n=1}^{N}\zeta_n l_n|h_n|^2(P_t - \exp(\tilde{\tau}_n+\tilde{P}_n))\\ &-\sum_{n=1}^{N}\lambda_n\left(\ln\left(2^{2r_{\text{th,n}}\exp(-\tilde{\tau}_n)}-1\right)-\ln\frac{el_n^2|h_n|^4}{2\pi\left(\sigma^2_{\text{rec,n}}+\sigma^2_{\text{ADC,n}}\right)}-2\tilde{P}_n\right)\\ &+\mu\left(P_t-\sum_{n=1}^{N}\exp(\tilde{\tau}_n+\tilde{P}_n)\right)+\nu\left(1-\sum_{n=1}^{N}\exp(\tilde{\tau}_n)\right),\end{aligned} \tag{84}$$

where λ_n, μ and ν denote the LMs. Determining the first derivative of the Lagrangian with respect to $\tilde{P}_n$ and $\tilde{\tau}_n$, respectively, yields the following analytic expressions

$$\frac{d\mathcal{L}}{d\tilde{P}_n} = 2\lambda_n - \exp(\tilde{\tau}_n+\tilde{P}_n)(\mu+\zeta_n l_n|h_n|^2) \tag{85}$$

and

$$\begin{aligned}\frac{d\mathcal{L}}{d\tilde{\tau}_n} =& -\exp(\tilde{\tau}_n)(\nu+\exp(\tilde{P}_n)(\mu+\zeta_n l_n|h_n|^2))\\ &+\frac{2\lambda_n 2^{2r_{\text{th,n}}\exp(-\tilde{\tau}_n)}r_{\text{th,n}}\exp(-\tilde{\tau}_n)\ln 2}{2^{2r_{\text{th,n}}\exp(-\tilde{\tau}_n)}-1}.\end{aligned} \tag{86}$$

Based on this and setting (85) to zero, it follows that

$$\exp(\tilde{P}_n) = \frac{2\lambda_n}{\mu+\zeta_n l_n|h_n|^2}\exp(-\tilde{\tau}_n), \tag{87}$$

from which (54) is derived. Also, setting (86) equal to zero and using (87), the following expression is deduced

$$\frac{\lambda_n\ln 2}{2r_{\text{th,n}}}2^{z_n}z_n^2 = \left(\nu+\frac{\lambda_n}{r_{\text{th,n}}}z_n\right)(2^{z_n}-1), \tag{88}$$

where

$$z_n = 2r_{\text{th,n}}\exp(-\tilde{\tau}_n), \tag{89}$$

which proves the validity of (55) and concludes the proof. It is noted here that the LMs in (54) and (56) are calculated iteratively by using the subgradient method [51], where positive step sizes are used and chosen in order to satisfy the diminishing step size. Since the optimization problem (53) is convex, it is guaranteed that the optimal solution is global and can be obtained in polynomial time.

REFERENCES

[1] S. A. Tegos, P. D. Diamantoulakis, K. Pappi, and G. K. Karagiannidis, "Optimal Simultaneous Wireless Information and Power Transfer with Low-Complexity Receivers," in *Proc. IEEE 19th International Workshop Signal Processing Advances in Wireless Communications (SPAWC)*, Jun. 2018, pp. 1–5.

[2] I. Krikidis, S. Timotheou, S. Nikolaou, G. Zheng, D. W. K. Ng, and R. Schober, "Simultaneous wireless information and power transfer in modern communication systems," *IEEE Commun. Mag.*, vol. 52, no. 11, pp. 104–110, Nov. 2014.

[3] L. R. Varshney, "Transporting information and energy simultaneously," in *Proc. IEEE International Symposium on Information Theory*, Jul. 2008, pp. 1612–1616.

[4] P. Grover and A. Sahai, "Shannon meets Tesla: Wireless information and power transfer," in *Proc. IEEE International Symposium on Information Theory*, Jun. 2010, pp. 2363–2367.

[5] D. W. K. Ng, T. Q. Duong, C. Zhong, and R. Schober, *Wireless Information and Power Transfer: Theory and Practice*. Wiley-IEEE Press, 2019.

[6] P. D. Diamantoulakis, G. K. Karagiannidis, and Z. Ding, "Simultaneous Lightwave Information and Power Transfer (SLIPT)," *IEEE Trans. Green Commun. Netw.*, vol. 2, no. 3, pp. 764–773, Sep. 2018.

[7] C. Zhong, H. A. Suraweera, G. Zheng, I. Krikidis, and Z. Zhang, "Wireless information and power transfer with full duplex relaying," *IEEE Trans. Commun.*, vol. 62, no. 10, pp. 3447–3461, Oct. 2014.

[8] S. Bi, C. K. Ho, and R. Zhang, "Wireless powered communication: Opportunities and challenges," *IEEE Commun. Mag.*, vol. 53, no. 4, pp. 117–125, Apr. 2015.

[9] H. Ju and R. Zhang, "Throughput maximization in wireless powered communication networks," *IEEE Trans. Wireless Commun.*, vol. 13, no. 1, pp. 418–428, Jan. 2014.

[10] P. D. Diamantoulakis, K. N. Pappi, Z. Ding, and G. K. Karagiannidis, "Wireless-powered communications with non-orthogonal multiple access," *IEEE Trans. Wireless Commun.*, vol. 15, no. 12, pp. 8422–8436, Dec. 2016.

[11] P. D. Diamantoulakis, K. N. Pappi, G. K. Karagiannidis, H. Xing, and A. Nallanathan, "Joint downlink/uplink design for wireless powered networks with interference," *IEEE Access*, vol. 5, pp. 1534–1547, Jan. 2017.

[12] Q. Wu, M. Tao, D. W. K. Ng, W. Chen, and R. Schober, "Energy-efficient resource allocation for wireless powered communication networks," *IEEE Trans. Wireless Commun.*, vol. 15, no. 3, pp. 2312–2327, Mar. 2016.

[13] P. D. Diamantoulakis and G. K. Karagiannidis, "Maximizing proportional fairness in wireless powered communications," *IEEE Wireless Commun. Lett.*, vol. 6, no. 2, pp. 202–205, Apr. 2017.

[14] D. Li, W. Peng, and Y. Liang, "Hybrid ambient backscatter communication systems with harvest-then-transmit protocols," *IEEE Access*, vol. 6, pp. 45 288–45 298, Aug. 2018.

[15] P. D. Diamantoulakis, G. D. Ntouni, K. N. Pappi, G. K. Karagiannidis, and B. S. Sharif, "Throughput maximization in multicarrier wireless powered relaying networks," *IEEE Wireless Commun. Lett.*, vol. 4, no. 4, pp. 385–388, Aug. 2015.

[16] D. W. K. Ng, E. S. Lo, and R. Schober, "Energy-efficient power allocation in OFDM systems with wireless information and power transfer," in *Proc. IEEE International Conference on Communications (ICC)*, Jun. 2013, pp. 4125–4130.

[17] D. W. K. Ng and R. Schober, "Spectral efficient optimization in OFDM systems with wireless information and power transfer," in *Proc. 21st European Signal Processing Conference (EUSIPCO)*, Sep. 2013, pp. 1–5.

[18] R. Zhang and C. K. Ho, "MIMO Broadcasting for Simultaneous Wireless Information and Power Transfer," *IEEE Trans. Wireless Commun.*, vol. 12, no. 5, pp. 1989–2001, May 2013.

[19] X. Chen, Z. Zhang, H. H. Chen, and H. Zhang, "Enhancing wireless information and power transfer by exploiting multi-antenna techniques," *IEEE Commun. Mag.*, vol. 53, no. 4, pp. 133–141, Apr. 2015.

[20] Z. Ding, C. Zhong, D. W. K. Ng, M. Peng, H. A. Suraweera, R. Schober, and H. V. Poor, "Application of smart antenna technologies in simultaneous wireless information and power transfer," *IEEE Commun. Mag.*, vol. 53, no. 4, pp. 86–93, Apr. 2015.

[21] Z. Xiang and M. Tao, "Robust beamforming for wireless information and power transmission," *IEEE Wireless Commun. Lett.*, vol. 1, no. 4, pp. 372–375, Jun. 2012.

[22] C. Zhong, X. Chen, Z. Zhang, and G. K. Karagiannidis, "Wireless-powered communications: Performance analysis and optimization," *IEEE Trans. Commun.*, vol. 63, no. 12, pp. 5178–5190, Dec. 2015.

[23] S. Timotheou, G. Zheng, C. Masouros, and I. Krikidis, "Exploiting constructive interference for simultaneous wireless information and power transfer in multiuser downlink systems," *IEEE J. Sel. Areas Commun.*, vol. 34, no. 5, pp. 1772–1784, May 2016.

[24] L. Mohjazi, I. Ahmed, S. Muhaidat, M. Dianati, and M. Al-Qutayri, "Downlink beamforming for SWIPT multi-user MISO underlay cognitive radio networks," *IEEE Commun. Lett.*, vol. 21, no. 2, pp. 434–437, Feb 2017.

[25] Y. Huang and B. Clerckx, "Relaying strategies for wireless-powered MIMO relay networks," *IEEE Trans. Wireless Commun.*, vol. 15, no. 9, pp. 6033–6047, Sep. 2016.

[26] X. Zhou, R. Zhang, and C. K. Ho, "Wireless information and power transfer in multiuser OFDM systems," *IEEE Trans. Wireless Commun.*, vol. 13, no. 4, pp. 2282–2294, Mar. 2014.

[27] Z. Ding, I. Krikidis, B. Sharif, and H. V. Poor, "Wireless information and power transfer in cooperative networks with spatially random relays," *IEEE Trans. Wireless Commun.*, vol. 13, no. 8, pp. 4440–4453, Aug. 2014.

[28] Z. Yang, Z. Ding, P. Fan, and G. K. Karagiannidis, "Outage performance of cognitive relay networks with wireless information and power transfer," *IEEE Trans. Veh. Technol.*, vol. 65, no. 5, pp. 3828–3833, May 2016.

[29] I. Krikidis, "Relay selection in cooperative networks with wireless battery charging," in *Proc. IEEE Global Communications Conference (GLOBECOM)*, Dec 2015, pp. 1–6.

[30] J. Ye, H. Lei, Y. Liu, G. Pan, D. B. da Costa, Q. Ni, and Z. Ding, "Cooperative communications with wireless energy harvesting over nakagami- m fading channels," *IEEE Trans. Commun.*, vol. 65, no. 12, pp. 5149–5164, Dec 2017.

[31] H. Ding, D. B. da Costa, H. A. Suraweera, and J. Ge, "Role selection cooperative systems with energy harvesting relays," *IEEE Trans. Wireless Commun.*, vol. 15, no. 6, pp. 4218–4233, Jun. 2016.

[32] Y. Ye, L. Shi, X. Chu, H. Zhang, and G. Lu, "On the Outage Performance of SWIPT-Based Three-Step Two-Way DF Relay Networks," *IEEE Trans. Veh. Technol.*, vol. 68, no. 3, pp. 3016–3021, Mar. 2019.

[33] H. Xing, K. K. Wong, A. Nallanathan, and R. Zhang, "Wireless powered cooperative jamming for secrecy multi-AF relaying networks," *IEEE Trans. Wireless Commun.*, vol. 15, no. 12, pp. 7971–7984, Dec. 2016.

[34] L. Liu, R. Zhang, and K. C. Chua, "Secrecy wireless information and power transfer with MISO beamforming," *IEEE Trans. Signal Process.*, vol. 62, no. 7, pp. 1850–1863, Apr. 2014.

[35] H. Xing, L. Liu, and R. Zhang, "Secrecy wireless information and power transfer in fading wiretap channel," *IEEE Trans. Veh. Technol.*, vol. 65, no. 1, pp. 180–190, Jan. 2016.

[36] B. Clerckx, "Wireless information and power transfer: Nonlinearity, waveform design, and rate-energy tradeoff," *IEEE Trans. Signal Process.*, vol. 66, no. 4, pp. 847–862, Feb. 2018.

[37] K. Xiong, B. Wang, and K. R. Liu, "Rate-energy region of SWIPT for MIMO broadcasting under nonlinear energy harvesting model," *IEEE Trans. Wireless Commun.*, vol. 16, no. 8, pp. 5147–5161, Aug. 2017.

[38] S. Wang, M. Xia, K. Huang, and Y. Wu, "Wirelessly powered two-way communication with nonlinear energy harvesting model: Rate regions under fixed and mobile relay," *IEEE Trans. Wireless Commun.*, vol. 16, no. 12, pp. 8190–8204, Dec. 2017.

[39] J. Kang, I. Kim, and D. I. Kim, "Wireless information and power transfer: Rate-energy tradeoff for nonlinear energy harvesting," *IEEE Trans. Wireless Commun.*, vol. 17, no. 3, pp. 1966–1981, Mar. 2018.

[40] B. Clerckx, R. Zhang, R. Schober, D. W. K. Ng, D. I. Kim, and H. V. Poor, "Fundamentals of wireless information and power transfer: From RF energy harvester models to signal and system designs," *IEEE J. Sel. Areas Commun.*, vol. 37, no. 1, pp. 4–33, Jan. 2019.

[41] X. Zhou, R. Zhang, and C. K. Ho, "Wireless information and power transfer: Architecture design and rate-energy tradeoff," *IEEE Trans. Commun.*, vol. 61, no. 11, pp. 4754–4767, Nov. 2013.

[42] L. Mohjazi, S. Muhaidat, M. Dianati, and M. Al-Qutayri, "Performance analysis of SWIPT relay networks with noncoherent modulation," *IEEE Trans. Green Commun. Netw.*, pp. 1–1, Dec. 2018.

[43] E. Goudeli, C. Psomas, and I. Krikidis, "Sequential decoding for simultaneous wireless information and power transfer," in *Proc. 24th International Conference Telecommunications (ICT)*, May 2017, pp. 1–5.

[44] C. H. Chang, R. Y. Chang, and F. T. Chien, "Energy-assisted information detection for simultaneous wireless information and power transfer: Performance analysis and case studies," *IEEE Trans. Signal Inf. Process. Netw.*, vol. 2, no. 2, pp. 149–159, Jun. 2016.

[45] Y.-b. Kim, D. K. Shin, and W. Choi, "Rate-energy region in wireless information and power transfer: New receiver architecture and practical modulation," *IEEE Trans. Commun.*, pp. 2751–2761, Feb. 2018.

[46] J. Rubio, A. Pascual-Iserte, D. P. Palomar, and A. Goldsmith, "Joint optimization of power and data transfer in multiuser MIMO systems," *IEEE Trans. Signal Process.*, vol. 65, no. 1, pp. 212–227, Oct. 2017.

[47] S. Neumark, *Solution of cubic and quartic equations*. Elsevier, 2014.

[48] Y. Ye, Y. Li, Z. Wang, X. Chu, and H. Zhang, "Dynamic asymmetric power splitting scheme for swipt-based two-way multiplicative af re-

laying," *IEEE Signal Process. Lett.*, vol. 25, no. 7, pp. 1014–1018, Jul. 2018.
[49] T. M. Cover and J. A. Thomas, *Elements of information theory*, 2nd ed. Wiley-Interscience, 2006.
[50] A. Lapidoth, S. M. Moser, and M. A. Wigger, "On the capacity of free-space optical intensity channels," *IEEE Trans. Inf. Theory*, vol. 55, no. 10, pp. 4449–4461, Oct. 2009.
[51] S. Boyd and L. Vandenberghe, *Convex optimization*. Cambridge University Press, 2004.

Sotiris A. Tegos was born in Serres, Greece. He received the Diploma Degree (5 years) in Electrical and Computer Engineering from the Aristotle University of Thessaloniki (AUTH), Greece, in 2018, where he is currently pursuing his PhD with the Department of Electrical and Computer Engineering. He was a visitor researcher at the department of Electrical and Computer Engineering at Khalifa University, Abu Dhabi, UAE. His current research interests include resource allocation in wireless communications, wireless power transfer, optimization theory and applications, and probability theory. He has served as a reviewer in various IEEE journals and conferences.

Dr. Panagiotis D. Diamantoulakis (SM 2018) received the Diploma Degree (5 years) and his PhD in Electrical and Computer Engineering from the Aristotle University of Thessaloniki (AUTH), Greece, in 2012 and 2017, respectively. His current research interests include resource allocation in wireless communications, optimization theory and applications, game theory, non-orthogonal multiple access, and wireless power transfer. He serves as Editor in the IEEE Wireless communications Letters and in Elsevier Physical Communication. Also, he was an exemplary reviewer in IEEE Communication Letters for 2014 and IEEE Transactions on Wireless Communications 2017 (top 3% of reviewers). Dr. Diamantoulakis is IEEE Senior Member.

Dr. Koralia N. Pappi has received the Diploma Degree (5 years) and her PhD in Electrical and Computer Engineering from the Aristotle University of Thessaloniki, Greece, in 2010 and 2015, respectively. In 2015 she joined the Intracom S.A. Telecom Solutions and the Ericsson Signaling Controller product development unit. Since 2015, she is also an adjunct post-doctoral researcher with the Wireless Communications Systems Group (WCSG) of the Department of Electrical and Computer Engineering, Aristotle University of Thessaloniki. She has received several exemplary reviewer awards from IEEE journals. Dr. Pappi serves as an associate editor of the IEEE Communications Letters since 2017.

Paschalis C. Sofotasios received the MEng degree from Newcastle University, the MSc degree from the University of Surrey and the PhD degree from the University of Leeds. He has held positions at the University of Leeds, University of California Los Angeles, Aristotle University of Thessaloniki, Tampere University of Technology and Khalifa University, where he is currently an Assistant Professor in the Department of Electrical Engineering and Computer Science. His research interests are in physical layer communications concerning both digital and optical wireless communications. He has received the best paper award at ICUFN 13, he has served as TPC co-chair or member in numerous IEEE conferences and he has received several exemplary reviewer awards from IEEE journals. Dr. Sofotasios is Editor for IEEE Communications Letters and a Senior Member of IEEE.

Sami Muhaidat received the Ph.D. degree in Electrical and Computer Engineering from the University of Waterloo, Waterloo, Ontario, in 2006. From 2007 to 2008, he was an NSERC postdoctoral fellow in the Department of Electrical and Computer Engineering, University of Toronto, Canada. From 2008-2012, he was an Assistant Professor in the School of Engineering Science, Simon Fraser University, BC, Canada. He is currently a Professor at Khalifa University, and a Visiting Professor in the Faculty of Engineering, University of Surrey, UK. The research interests of Dr. Muhaidat focus on wireless communications, optical communications, IoT with emphasis on battery-less devices, and machine learning. He is currently an Area Editor for IEEE Transactions on Communications. He served as a Senior Editor for IEEE Communications Letters, an Editor for IEEE Transactions on Communications, and an Associate Editor for IEEE Transactions on Vehicular Technology. He is also a member of Mohammed Bin Rashid Academy of scientists.

Dr. George K. Karagiannidis (M96-SM03-F14) was born in Pithagorion, Samos Island, Greece. He received the University Diploma (5 years) and PhD degree, both in electrical and computer engineering from the University of Patras, in 1987 and 1999, respectively. From 2000 to 2004, he was a Senior Researcher at the Institute for Space Applications and Remote Sensing, National Observatory of Athens, Greece. In June 2004, he joined the faculty of Aristotle University of Thessaloniki, Greece where he is currently Professor in the Electrical and Computer Engineering Dept. and Director of Digital Telecommunications Systems and Networks Laboratory. He is also Honorary Professor at South West Jiaotong University, Chengdu, China. His research interests are in the broad area of Digital Communications Systems and Signal processing, with emphasis on Wireless Communications, Optical Wireless Communications, Wireless Power Transfer and Applications, Communications for Biomedical Engineering, Stochastic Processes in Biology and Wireless Security. He is the author or co-author of more than 500 technical papers published in scientific journals and presented at international conferences. He is also author of the Greek edition of a book on Telecommunications Systems and co-author of the book Advanced Optical Wireless Communications Systems, Cambridge Publications, 2012. Dr. Karagiannidis has been involved as General Chair, Technical Program Chair and member of Technical Program Committees in several IEEE and non-IEEE conferences. In the past, he was Editor in IEEE Transactions on Communications, Senior Editor of IEEE Communications Letters, Editor of the EURASIP Journal of Wireless Communications and Networks and several times Guest Editor in IEEE Selected Areas in Communications. From 2012 to 2015 he was the Editor-in Chief of IEEE Communications Letters. Dr. Karagiannidis is one of the highly-cited authors across all areas of Electrical Engineering, recognized from Clarivate Analytics as Web-of-Science Highly-Cited Researcher in the four consecutive years 2015-2018.